Dynamics of a quantum phase transition in the Aubry-André-Harper model with *p*-wave superconductivity

Xianqi Tong,[1] Ye-Ming Meng,[1] Xunda Jiang,[2] Chaohong Lee,[2,3] Gentil Dias de Moraes Neto,[1] and Gao Xianlong[1,*]

[1]*Department of Physics, Zhejiang Normal University, Jinhua 321004, People's Republic of China*

[2]*Guangdong Provincial Key Laboratory of Quantum Metrology and Sensing & School of Physics and Astronomy, Sun Yat-Sen University (Zhuhai Campus), Zhuhai 519082, China*

[3]*State Key Laboratory of Optoelectronic Materials and Technologies, Sun Yat-Sen University (Guangzhou Campus), Guangzhou 510275, China*

(Received 22 December 2020; revised 26 February 2021; accepted 1 March 2021; published 10 March 2021)

We investigate the nonequilibrium dynamics of the one-dimension Aubry-André-Harper model with *p*-wave superconductivity by changing the potential strength with slow and sudden quench. Firstly, we study the slow quench dynamics from the localized phase to the critical phase by linearly decreasing the potential strength V. The localization length is finite and its scaling obeys the Kibble-Zurek mechanism. The results show that the second-order phase transition line shares the same critical exponent $z\nu$, giving the correlation length $\nu = 1$ and dynamical exponent $z = 1.373 \pm 0.023$, which are different from the Aubry-André model. Secondly, we also study the sudden quench dynamics between three different phases: localized phase, critical phase, and extended phase. In the limit of $V = 0$ and $V = \infty$, we analytically study the sudden quench dynamics via the Loschmidt echo. The results suggest that, if the initial state and the post-quench Hamiltonian are in different phases, the Loschmidt echo vanishes at some time intervals. Furthermore, we found that, if the initial value is in the critical phase, the direction of quenching is the same as one of the two limits mentioned before, and similar behaviors will occur.

DOI: 10.1103/PhysRevB.103.104202

I. INTRODUCTION

In recent years, extensive research has been carried out to unravel the behavior of quasiperiodic structures [1–6]. The quasiperiodic system, being aperiodic but deterministic, lacks translational invariance but shows long-range order leading to a rich critical behavior [1,2,7–10]. The critical properties are different or can be regarded as intermediate from those of ordinary (periodic) and disordered (random) systems. For instance, the spatial modulation of the parameters can change the universality class of a quantum phase transition, i.e., the critical exponents that characterized the equilibrium properties of the physical observables at the transition point [11–13]. Furthermore, one-dimensional quasiperiodic systems, known as the Aubry-André-Harper (AAH) model [1,5,6,12,14–22], show the Anderson localization transition [23] at a finite strength of the quasiperiodic disorder that differs from the original one-dimensional random model.

In the AAH model, the states at the critical point are neither extended nor localized but critical, characterized by power-law localization, and fractal-like spectrum and wave functions [22,24]. In an interacting system, the many-body localization with random or quasiperiodic case exhibit quite different behaviors [25]. Furthermore, the quantum phase transitions of quasiperiodic system related to quantum magnetism described by spin Hamiltonians [26–35] and respective fermionic counterparts [14,36], were studied extensively. In particular, the anisotropic XY chain in a transverse magnetic field [37–43], that maps via Jordan-Wigner transformation, to the AAH model with *p*-wave superconducting (SC) pairing terms [14,36], and contains the quantum Ising and XY chains as limiting cases, has drawn attention for a rich phase diagram, as depicted in Fig. 1. The anisotropy (SC pairing) destroys the self-duality of the isotropic XY model and stabilizes the critical phase sandwiched between extended and localized phases.

Although the phase diagram of the AAH model with SC pairing is well understood [22], it lacks the thorough investigation of the critical behavior and the nonequilibrium dynamics. Specifically, in a continuous phase transition, the correlation length ξ diverges at the transition as $\xi \approx \epsilon^{-\nu}$ and the corresponding gap Δ goes zero as $\Delta \approx \xi^{-z}$, where ϵ is the distance from the critical point, ν and z are the correlation length and dynamical critical exponents. To the best of our knowledge, there is no report in literature about the critical exponents of the AAH model with SC pairing.

In this context, it is important to determine the nonequilibrium dynamical signatures of a quantum phase transition [44–59], which has also been explored in a quasiperiodic system both experimentally [60–62] and theoretically [26–29,63–67]. It is useful to discriminate between two limiting processes of slowly and instantaneously changing of the parameters. Driving the parameter across the second-order phase transition is usually described by the Kibble-Zurek mechanism (KZM) [68–70]. The essence of the KZM is the breaking of

*Corresponding author: gaoxl@zjnu.edu.cn

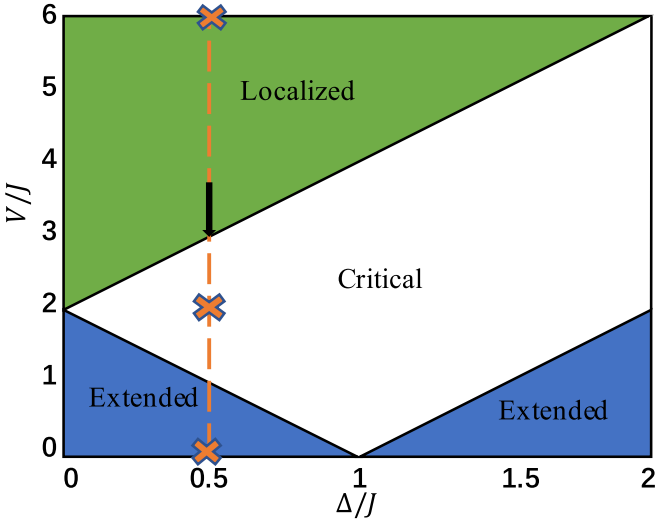

FIG. 1. Sketch of the phase diagram of the AAH model with p-wave superconducting paring order parameter Δ and the disorder strength V [22]. Three different phases, that is, extended phase, critical phase, and localized phase are shown up in different parameter regimes. The line between critical phase and localized phase is a second-order phase transition line. The vertical line at $\Delta = 0.5$ passing through three different phases indicates the cases we studied. The KZM as indicated by the solid arrow is studied in Fig. 4, and the quenching as indicated by the crosses mark is studied in Figs. 6 and 7.

the adiabaticity for crossing the critical point of a quantum phase transition, which leads to the corresponding excitations following a power law relation with respect to the quench rate [71,72]. For the dynamical quantum phase transition, the quantum system is quenched out of equilibrium by suddenly changing the parameters of the Hamiltonian. For the sudden quench dynamics, Loschmidt echo is an important quantity, which measures the overlap between the initial state and the time-evolved state [50–53]. Many theoretical works have demonstrated that the Loschmidt echo plays a significant role in characterizing the nonequilibrium dynamical signature of the quantum phase transition [44–46,51]. Recently, thanks to the developments of the quantum simulation techniques, the dynamical quantum phase transition can be directly detected in a string of ions simulating the interacting transverse field Ising model [73].

However, the time evolution of the Loschmidt echo and the KZM requires an in-depth investigation in a one-dimensional quasiperiodic system which reveal phase transitions among localized phase, critical phase, and extended phase. Here, we pay attention to such a quantum disordered system described by the AAH model with p-wave SC paring [22,24,74–77].

The rest of the paper is organized as follows. In Sec. II, we explicitly write down the Schrödinger equation of the one-dimensional quasiperiodic system induced by the on-site incommensurate potential. In Sec. III, we calculate the critical exponents and verify the KZM hypothesis. In Sec. IV, we discuss the sudden quench dynamics of the quantum phase transition between different phases and give the analytical expressions of two limits cases. Section V is devoted to our conclusion.

II. MODEL HAMILTONIAN

The generalized one-dimensional AAH model with p-wave SC paring is described by the following Hamiltonian:

$$H = \sum_{j=1}^{N} V_j c_j^\dagger c_j + j \sum_{j=1}^{N-1} (-J c_{j+1}^\dagger c_j + \Delta c_{j+1}^\dagger c_j^\dagger + \text{H.c.}), \quad (1)$$

where c_j ($c_j^\dagger$) is the fermionic annihilation (creation) operator at the j-th site. Here $V_j = V\cos(2\pi\alpha j + \phi)$ is the incommensurate potential with $\alpha = (\sqrt{5}-1)/2$ being an irrational number, which is a deterministic quasiperiodic one. V is the strength of the incommensurate potential, and the random phase $\phi \in [0, 2\pi)$ is employed in the case where it is necessary to average over the pseudorandom potential. J is the nearest-neighbor hopping amplitude and we set $J = 1$ as energy unit throughout this paper. Δ is the amplitude of the p-wave SC paring. The phase diagram of this system has three different phases shown in Fig. 1: the localized phase, critical phase, and extended phase, which are marked by green, white, and blue, respectively. For $V = 2|J + \Delta|$, the system undergoes a second-order phase transition from critical phase to localized phase [74]. For $V = 2|J - \Delta|$, the system has a phase transition from critical phase to extended phase [22,24]. Firstly, we need to rewrite the Hamiltonian by using the Bogoliubov–de Gennes transformation,

$$\eta_n^\dagger = \sum_{j=1}^{N} [u_{n,j} c_j^\dagger + v_{n,j} c_j], \quad (2)$$

where $n = 1, ..., N$, the Bogoliubov modes $(u_{n,j}, v_{n,j})$ are the eigenstates of the Hamiltonian and $u_{n,j}, v_{n,j}$ are chosen be real, so the Hamiltonian can be diagonalized as

$$H = \sum_{n=1}^{N} \varepsilon_n \left(\eta_n^\dagger \eta_n - \frac{1}{2}\right), \quad (3)$$

with ε_n being the spectrum of quasiparticles. For the n-th Bogoliubov modes, we have the following Bogoliubov–de Gennes equations:

$$\begin{aligned} -Ju_{j-1} + \Delta v_{j-1} + V_j u_j - Ju_{j+1} - \Delta v_{j+1} &= \varepsilon u_j, \\ -\Delta u_{j-1} + Jv_{j-1} - V_j v_j + \Delta u_{j+1} + Jv_{j+1} &= \varepsilon v_j. \end{aligned} \quad (4)$$

The wave function is expressed as

$$|\Psi_n\rangle = [u_{n,1}, v_{n,1}, u_{n,2}, v_{n,2}, ..., u_{n,N}, v_{n,N}]^T, \quad (5)$$

then for the Schrödinger equation $H|\Psi_n\rangle = \varepsilon_n|\Psi_n\rangle$, the Hamiltonian can be written as a $2N \times 2N$ matrix:

$$H = \begin{pmatrix} A_1 & B & 0 & \dots & \dots & \dots & C \\ B^\dagger & A_2 & B & 0 & \dots & \dots & 0 \\ 0 & B^\dagger & A_3 & B & 0 & \dots & 0 \\ \vdots & \ddots & \ddots & \ddots & \ddots & \ddots & \vdots \\ 0 & \dots & 0 & B^\dagger & A_{N-2} & B & 0 \\ 0 & \dots & \dots & 0 & B^\dagger & A_{N-1} & B \\ C^\dagger & \dots & \dots & \dots & 0 & B^\dagger & A_N \end{pmatrix}, \quad (6)$$

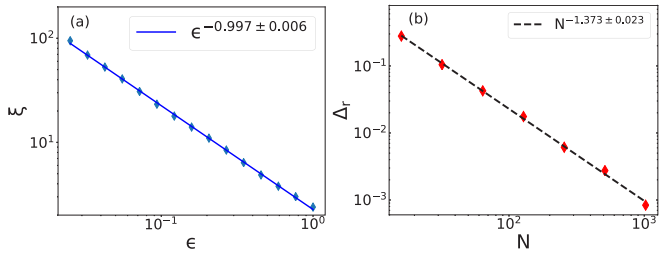

FIG. 2. (a) The localization length ξ as a function of the distance from the critical point $\epsilon = V - V_c$. Here ξ was calculated by using the ground state of the corresponding Hamiltonian. The linear fit $\xi \sim \epsilon^{-\nu}$ yields correlation-length exponent $\nu = 0.997 \pm 0.006$; cf. Eq. (10). (b) The relevant gap Δ_r which is the sum of two lowest eigenenergies at the critical point as a function of N. Fitting $\Delta_r \sim N^{-z}$ yields a dynamical exponent $z = 1.373 \pm 0.023$; see Eq. (11). Here, we set SC pairing amplitude $\Delta = 0.5$, the critical point $V_c = 3$, and the lattice size $N = 987$ in (a). Averaging is done over 200 random values of ϕ.

where

$$A = \begin{pmatrix} V_j & 0 \\ 0 & -V_j \end{pmatrix}, \tag{7}$$

$$B = \begin{pmatrix} -J & -\Delta \\ \Delta & J \end{pmatrix}, \tag{8}$$

and

$$C = \begin{pmatrix} -J & \Delta \\ -\Delta & J \end{pmatrix}. \tag{9}$$

Here, we assume the Hamiltonian with periodic boundary condition, hence α can be approximated by a rational number with L in the denominator. Dependence of L implies an order $L = F_m$, $\alpha = F_{m-1}/F_m$, where the F_m is a Fibonacci number.

III. KIBBLE-ZUREK MECHANISM

When V is gradually decreased to approach the critical point, correlation length will diverge as

$$\xi \approx \epsilon^{-\nu}, \quad \epsilon = V - V_c, \tag{10}$$

where ϵ is the distance from the critical point and $\nu = 0.997 \pm 0.006$ is a correlation-length exponent extracted from Fig. 2(a), consistent with the predicted $\nu = 1$ [78] within the numerical accuracy. Without loss of generality, we choose $\Delta = 0.5$ in the text. We test numerically in Appendix B that the correlation exponent and the correlation length for different critical points on the second-order phase transition line are the same within error bars.

The dynamic exponent z can be determined by the finite-size scaling of the relevant gap at the critical point, i.e., $\Delta_r = \varepsilon_0 + \varepsilon_1$, which is the sum of energies of the two positive lowest energy quasiparticles [79–81]:

$$\Delta_r \sim N^{-z}. \tag{11}$$

We use the linear fit to log-log plot of Fig. 2(b) which yields $z = 1.373 \pm 0.023$. The dynamical exponents $z\nu$ determine how the gap vanishes with the distance from the critical point. These critical exponents can be obtained from the study of the the fidelity susceptibility [82] and scaling analysis of superfluid fraction for different lattice sizes [83]. The whole results are also true for other points on the second-order phase transition line, except for the limited conditions of $\Delta = 0, -1$. When $\Delta = 0$, the Aubry-André model with p-wave superconductivity will return to the Aubry-André model [64]. When $\Delta = -1$, the model will return to quasiperiodic Ising model [78,84].

The initial state is deeply prepared in the localized state, and the potential V is slowly changed across the critical point between the critical and the localized phase.

Near the critical point, ϵ can be approximated by a linear quench:

$$\epsilon \approx -\text{sign}\,(t)\left|\frac{t}{\tau_Q}\right|, \tag{12}$$

here τ_Q is the quench time. The nonlinear quench is tested in Appendix C [85–87]. When the state is far away from the critical point, the state is adiabatically evolving. Then, the state crosses the adiabatic region to the diabatic region at a time point of its reaction time $\tau \sim \frac{1}{\Delta_r(t)} \sim |\frac{t}{\tau_Q}|^{-z\nu}$ equals the time scale $|\epsilon/\dot{\epsilon}|$. Thus there exists an intersection in which two timescales are equal, $t = \pm\hat{t}$, where

$$\hat{t} \sim \tau_Q^{z\nu/(1+z\nu)}. \tag{13}$$

The time-dependent state is still at the ground state until $t = -\hat{t}$ and $\hat{\epsilon} = \frac{\hat{t}}{\tau_Q} \sim \tau_Q^{-1/(1+z\nu)}$, with finite localization length

$$\hat{\xi} \sim \hat{\epsilon}^{-\nu} \sim \tau_Q^{\frac{\nu}{1+z\nu}}. \tag{14}$$

In zero-order approximation, the two time points $\pm\hat{t}$ divide the whole evolution into three regimes. Initially, when $t < -\hat{t}$, the state can adjust to the change of the Hamiltonian. However, at $t = -\hat{t}$ this tracking will cease, and the wave packet does not follow the instantaneous ground state until $\hat{t}$ with a finite localization length $\hat{\xi}$. Afterwards, it is the initial state for the adiabatic process that begins at $\hat{t}$ which is similar to the one "frozen out" at $-\hat{t}$.

However, we should also remember that such a "frozen out" instant is only a feasible hypothesis, but it is very helpful to deduce the scaling law. Actually, in a realistic system a sudden change does not exist at a certain moment during the evolution, which is a process from the adiabatic to the diabatic regime. Therefore, we can numerically test the KZM hypothesis by solving the critical dynamics, and estimate the frozen instant when the adiabaticity breaks. In this connection, although there is no unique way to quantify adiabatic loss, we use the fidelity $F(t)$ to describe the loss of adiabaticity, which provides a good approximation [88]

$$F(t) = |\langle\psi(t)|\Psi_0(t)\rangle|, \tag{15}$$

where $\langle\psi(t)|$ is the time-evolved state, and $|\Psi_0(t)\rangle$ is the instantaneous ground state. In Fig. 3, we plot the time-dependent fidelity $F(t)$ as a function of ϵ for four different quench rates, and the fidelity $F(t)$ decreases dramatically at the critical point [89]. From this, we can get the estimated values of the "frozen out" instants. The blue circle, orange square, green triangle, red hexagon represent the instants with different τ_Q. It is clearly shown that the corresponding "frozen

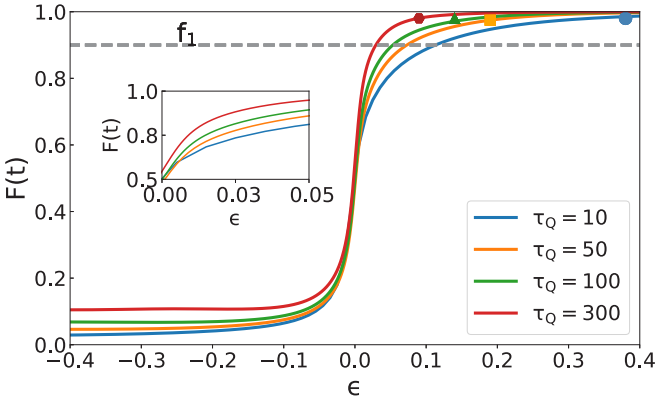

FIG. 3. The fidelity as a function of ϵ for four different $\tau_Q = 10, 50, 100, 300$, and the straight line $f_1 = 0.9$. The blue circle, orange square, green triangle, and red hexagon represent four corresponding "frozen out" instants. Inset: Enlarged view of ϵ between 0 and 0.05. The parameters are chosen as $\Delta = 0.5$, $V_c = 3$ and $N = 987$.

out" instant is closer to the critical point as the τ_Q increases. We choose one value represented by the straight line $f_1 = 0.9$, and we can see the fidelity in the four different instants are very close to 1 and away from 0.9. So until the instants, the loss of the adiabaticity is almost zero. But after that, the fidelity tends to fall faster, as shown in Fig. 3.

A. KZ POWER LAWS

In order to test the KZ scaling, we use smooth tanh profile $\epsilon(t) = -\tanh(t/\tau_Q)$ starting from $-5\tau_Q$ for the sake of suppressing excitation derived from the initial discontinuity of the time derivative $\dot{\epsilon}$ at $-5\tau_Q$.

When the system's evolution crosses the adiabatic area at $-\hat{t}$, then in the diabatic area, the finite localization length $\hat{\xi}$ does not change under the zero-order approximation until the time at $\hat{t}$. In Fig. 4, we plot $\hat{\xi}$ estimated by the dispersion of the probability distribution with three different system sizes of

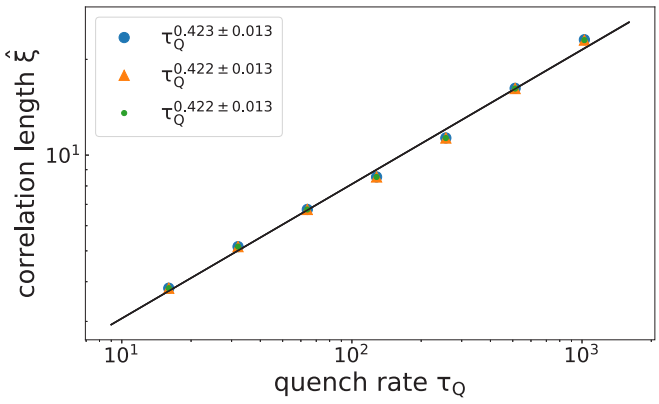

FIG. 4. The width of the wave packet as a function of the quench time τ_Q at the critical point under three different system sizes $N = 610, 987$, and 1597, respectively. The fitted straight line gives the $\hat{\xi} = \tau_Q^{0.423\pm0.013}$, $\tau_Q^{0.422\pm0.013}$, and $\tau_Q^{0.422\pm0.013}$, corresponding to $N = 610, 987$, and 1597, respectively; cf. Eq. (14). The parameters are chosen as $N = 987$, $\Delta = 0.5$, $V_c = 3$, and $\phi = 0$.

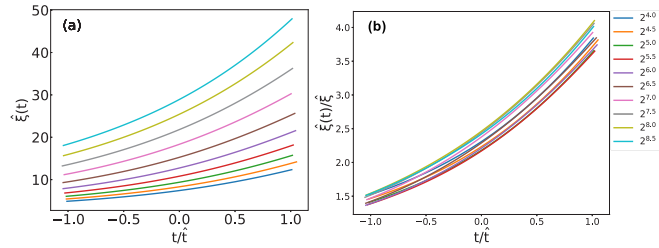

FIG. 5. In (a), the width of the wave packet $\hat{\xi}(t)$ as a function of the scaled time $-\hat{t}$ and $\hat{t}$ which represents the impulse regime. In (b), the scaled width of the wave packet $\hat{\xi}(t)/\hat{\xi}$ and scaled time all collapse to their respective scaling function. The parameters are chosen as in Fig. 4.

$N = 610, 987$, and 1597 as a function of τ_Q at the critical point $\epsilon = 0$. The fits of different sizes are all overlapped, indicating that the results have converged. The power-law fitting implies $z = 1.367$ according to the $\nu = 0.997$ estimated in Fig. 2(a) (while $z = 1.370$ for the $\nu = 1$).

A similar calculation for different critical points is shown in Appendix B, indicating that the correlation exponent and the correlation length on the second-order phase transition line are the same within error bars. We also discuss the dynamical scaling of the localization length at the critical point by taking the generalized nonlinear power law protocols, shown in Appendix C.

The dynamical exponent $z = 1.367$ extracted from the $\hat{\xi}$ in Fig. 4 differs from the $z \simeq 1.373$ obtained from the finite-size scaling in Fig. 2(b) by 0.6%. Similarly, the critical exponent $\nu \simeq 0.997$ is also 0.3% away from the value $\nu = 1$. The difference is almost the same as the system error. Therefore, within a small error range, our numerical results are consistent with the predicted results.

In the impulse area, $\hat{\xi}$ is the relevant scale of length. When $\tau_Q \to \infty$, the adiabatic limited is recovered. $\hat{\xi}$ diverges in the limit and becomes the only relevant scales in the long-wavelength regime. This logic proves the KZ scaling hypothesis [90–92] for a correlation length $\hat{\xi}(t)$ in the diabatic regime:

$$\hat{\xi}(t) = \hat{\xi} F_\xi(t/\hat{t}), \tag{16}$$

where F_ξ is a not a universal function as shown in Fig. 5.

IV. LOSCHMIDT ECHO

In the following section, we discuss another nonequilibrium dynamics by suddenly quenching the on-site potential V, not only between the localization phase and critical phase separated by the second-order phase transition line, but also between the critical phase and extended phase.

By preparing the initial state as the eigenstate of the Hamiltonian $H(V_i)$, and then suddenly quenching the Hamiltonian to $H(V_f)$, we calculate the return probability (Loschmidt echo) [93]:

$$L(t, V_i, V_f) = |G(t, V_i, V_f)|^2, \tag{17}$$

where $G(t, V_i, V_f)$ is the return amplitude (a type of Loschmidt echo amplitude):

$$G(t, V_i, V_f) = \langle\psi(V_i)|e^{-itH(V_f)}|\psi(V_i)\rangle, \tag{18}$$

where $\psi(V_i)$ is the eigenstate of the initial Hamiltonian $H(V_i)$, and V_i (V_f) represents the strength of the initial (final) incommensurate potential. The initial state is chosen to be the ground state of the initial Hamiltonian, and the results are also true for all the other eigenstates.

Then, we illustrate whether the zero points of the Loschmidt echo can be regarded as the signature of the phase transition among the localized phase, critical phase, and extended phase. To give a more intuitive explanation, we should consider two limiting cases. For these two cases, the initial value of V_i is set to $0(\infty)$ and $V_f = \infty(0)$ which can be calculated analytically, whereas the other cases are studied by the numerical methods.

If $V_i = 0$, the eigenvalues of the Hamiltonian are $\varepsilon_k = 2\sqrt{(J\cos ka)^2 + (\Delta \sin ka)^2}$, and the corresponding eigenstates are plane wave states $|\phi_k(V_i = 0)\rangle = \frac{e^{-i\pi/4}}{\sqrt{N}} \sum_{j=1}^{N} e^{ikj} c_j^\dagger |0\rangle$. If $V_f = \infty$, the system is in the localized phase, the eigenstates of the Hamiltonian are the localized states $|\Psi_n(V_f = \infty)\rangle = \sum_{j=1}^{N} \delta_{jn} c_j^\dagger |0\rangle$ with the eigenvalues $\varepsilon_n = V_f \cos(2\pi\alpha n)$. Then substituting the above results into Eq. (18), we can get the analytical solution $G_k = J_0(V_f t)$ [see Appendix A], where the $J_0(V_f t)$ is the zero-order Bessel function. It has a number of zeros x_n with $n = 1, 2, 3, ...$ These zeros mean that the Loschmidt amplitude and the echo can reach zeros at times:

$$t_n^* = \frac{x_n}{V_f}. \tag{19}$$

According to the dynamical quantum phase transition theory, the appearance of the zero points in Loschmidt echo can be regarded as the characteristics of the dynamical quantum phase transition and it is related to the divergence of the boundary partition function. Because the transition time t_n^* is inversely proportional to V_f, the Loschmidt echo oscillates faster with the increasing V_f. Then, if we rescale the time t to $V_f t$ as shown in Figs. 6(b)–6(f), the evolution of the Loschmidt echo shows similar behaviors for the quenching process of different V_f as shown in Figs. 6(b) and 6(c). The initial strength V_i is set to 0 and the SC paring $\Delta = 0.5$. It is apparent that the Loschmidt echo for $V_f = 2.2, 2.4, 2.6, 2.8$ in the critical phase or $V_f = 15, 30, 45, 60$ in the localized phase oscillates with different frequencies. However they are all quite similar after rescaling the time t to $V_f t$. Except for $V_f = 15$, in the localized phase, the numerical results almost coincide with the analytical solution shown in Fig. 6(c). Therefore, although the analytical solution is under the condition of $V_f \to \infty$, but the above result also holds true when V_f is large enough as shown in Fig. 6. To see the zero point in Loschmidt echo more clearly, we can calculate the "dynamical free energy" which is defined as $f(t) = -\log|G(t)|^2$. $f(t)$ is divergent at the time point when $t = t_n^*$ [44,45]. In Figs. 6(d) and 6(e), $f(t)$ is plotted as a function of different $V_f t$ with V_f in the localized phase or in the critical phase. Obviously it reaches the peaks at the critical times t_n^*, especially when V_f gets closer to the ∞.

In Fig. 6(f), we calculate the $L(t)$ as a function of the scaled time $V_f t$ with a series of final value taken in different phases.

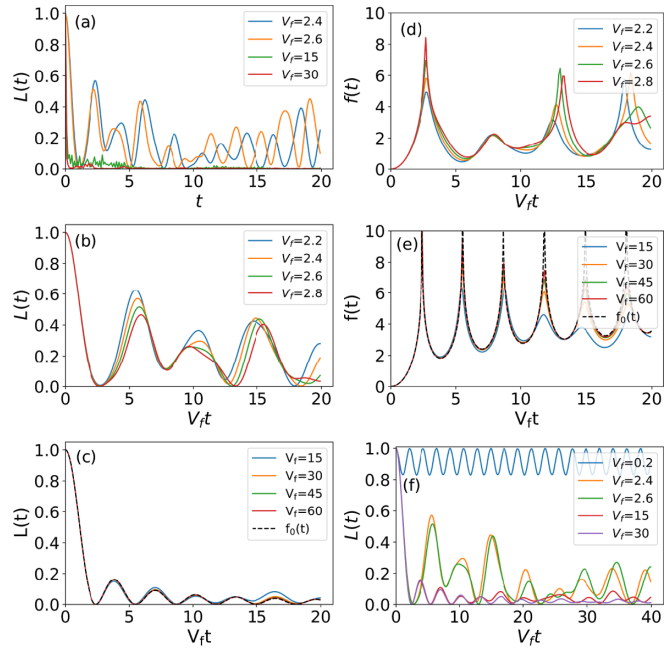

FIG. 6. The evolution of the Loschmidt echo with different t or $V_f t$. The system size $N = 987$ and the SC pairing $\Delta = 0.5$. The initial state is set to be the ground state of the Hamiltonian with $V_i = 0$. (a) Loschmidt echo versus t. (b) and (c) $L(t)$ versus different rescaled time $V_f t$. (d) and (e) "dynamic free energy" $f(t)$ versus $V_f t$. The $f_0(t) = -\log|J_0(V_f t)|^2$ is depicted by the black dotted line. (f) The evolution of the Loschmidt echo for various V_f including the extended, critical, localized phases. The Loschmidt echo will approach zero at some different time points. And it has different frequencies for different phases.

When $V_f < 2|J - \Delta|$, the Loschmidt echo cannot reach zero even for long time evolution, because V_i and V_f are in the same phase. However, when the final value V_f is in the critical phase or in the localized phase, $L(t)$ shows similar oscillations with different Δ_f and reaches zero. And the time interval of the Loschmidt echo has different ways for approaching the zero points in the critical and localized phase. By noticing that the condition of $V_f \to \infty$ cannot be met in the critical phase, and the analytical result $J_0(V_f t)$ is no longer applicable.

For the quenching process from a strong disorder strength V_i to $V_f = 0$. The system is initially prepared in the eigenstate of the localized phase, then is quenched into the extended regime. Similar to the above analysis [see Appendix A], we get the Loschmidt amplitude $G_n = J_0(2Jt)$, so the zero points of the Loschmidt echo appear at times

$$t_n^* = \frac{x_n}{2J}, \tag{20}$$

which is inversely proportional to the hopping amplitude $2J$, and different from Eq. (19). The transition time t_n^* is independent of V_f which means that for different V_f and the dynamical free energy has almost the same behaviors. Moreover, the return amplitude is insensitive to V_i, as long as V_i is large enough, even in the critical phase.

In Fig. 7, the Loschmidt echo and the dynamical free energy $f(t)$ as a function of the scaled time $V_f t$ or time t. But different from Fig. 6, the initial system here is in the

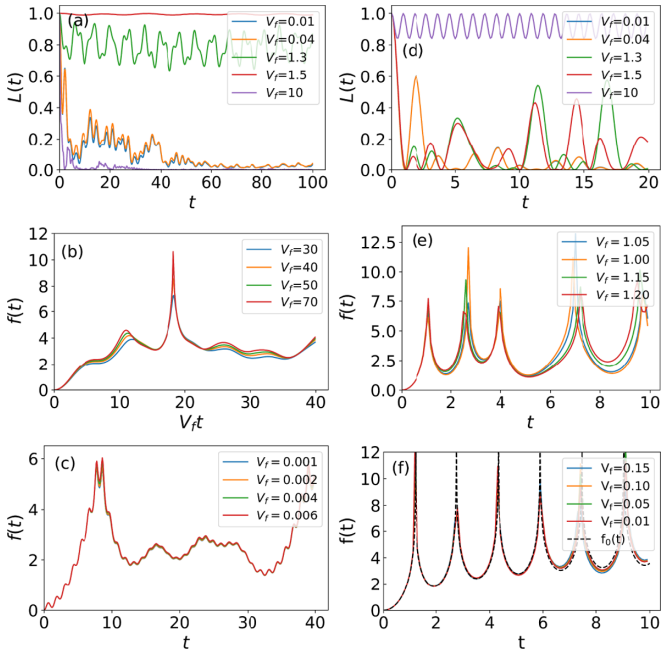

FIG. 7. The evolution of the Loschmidt echo with different $V_f t$ and t. The system size $N = 987$, the SC pairing $\Delta = 0.5$, and the initial state is set to the ground eigenstate of the Hamiltonian of $V_i = 2.6$ for (a), (b), and (c), but of $V_i = 100$ (d), (e), and (f). The initial state is the ground state of the Hamiltonian. (a) Loschmidt echo versus t; (b) and (c) $f(t)$ versus different rescaled time $V_f t$ and time t; (d) The evolution of the Loschmidt echo for various t. (e) and (f) "dynamic free energy" $f(t)$ versus t. The black dotted line corresponds to $f_0(t) = -\log|J_0(2Jt)|^2$ and the SC pairing $\Delta = 0.05$. In Figs (d), (e), and (f), the initial states are all in the localized phase. When $V_f < 1$, the Loschmidt echo will approach zero at the same time interval which is independent of V_f.

critical phase or localized phase. In the left panel of Fig. 7, the initial state is prepared in the critical phase, and in the right panel of Fig. 7, the initial state is set in the localized phase. Therefore, it is different from the previous analytical, when $V_i = 2.6$ and yet $V_f \gg 3$, we rescale the t to $V_f t$, but it is not needed when $V_f \ll 1$ shown in Fig. 7. In Fig. 7(a), we set $V_i = 2.6$ with $V_f = 0.01, 0.04, 1.3, 1.5, 10$, as long as $V_f < 2|J - \Delta|$ or $V_f > 2|J + \Delta|$ the Loschmidt echo will approach zero immediately, but when $V_f = 1.3, 1.5$ in the critical phase, $L(t)$ will never approach zero during the time evolution. In Fig. 7(b), $f(t)$ also shows similar behavior for different V_f after rescaling the time t to $V_f t$, due to the final value of the potential $V_f \gg V_i$. But the shape of the curve is different from $J_0(2Jt)$, because the initial state is in the critical phase. For Fig. 7(c), the same reason leads to mismatch between the peak shape and $J_0(2Jt)$. In analog to $V_i = 2.6$, we set $V_i = 100$ and take a series of V_f. We find that the Loschmidt echo approaches zero when $V_f < 2|J + \Delta|$ and it is also true for $V_f < 2|J - \Delta|$ in Figs. 7(d)–7(f). From Figs. 7(e) and 7(f), for V_f in the critical phase and extended phase, respectively, $f(t)$ shows similar behaviors. In Fig. 7(f), when the SC paring $\Delta = 0.05$, the behaviors of $f(t)$ with different V_f almost coincide with the analysis result $J_0(2Jt)$. As a result, when V_f approaches the limit of $V_f = 0$, the analytical result $G_n = J_0(2Jt)$ is a good approximation.

V. CONCLUSION

In summary, we have studied the different nonequilibrium dynamics of the AAH model with p-wave superconductivity in two different ways. Firstly, a linear ramp crossing the localization-critical phase transition line is not adiabatic, then from the linear fitting of the finite localization length near the critical point, we obtain the critical exponents $z\nu$ with $\nu = 0.997$ the same as Aubry-André model, and the dynamical exponent $z = 1.373$ different from Refs. [64,82,83]. Except for the point $\Delta = 0$, the critical exponents are almost the same at the second-order phase transition line $V = 2|J + \Delta|$. We also experiment with a series of different quenching directions, and the critical exponents are the same as what we got. Furthermore, we show $\hat{\xi}(t)$ as a function of τ_Q at the phase transition point, and we also show $\hat{\xi}(t)$ and $\hat{\xi}(t)/\hat{\xi}$ with different τ_Q but within the impulse regime $-\hat{t}$ and $\hat{t}$. The results are all consistent with the KZM scaling hypothesis. Our results indicate that KZM dominates the nonadiabatic dynamics of the one-dimensional incommensurate system with the localized-critical phase transition.

Next, we use the Loschmidt echo to study the sudden quench dynamics of the time evolution of the AAH model with p-wave SC pairing. The results show that the Loschmidt echo reaches zero as long as the initial and the final system are not in the same phases, which is also true for the critical phase. Especially, if V_i is in the critical phase, $L(t)$ and $f(t)$ show similar behaviors when the change of V has the same direction as the two limit cases mentioned before [94]. Our research results indicate that the zeros of the Loschmidt echo give the dynamic characteristics in the incommensurate system including the localized phase, critical phase, and extended phase.

Addressing some interesting issues to be investigated further, we first observe that the role played by incommensurability, i.e., by the irrational number α on the quasiperiodic potential was only slightly explored. It has been known that α determines the universality class and exotic non-power-law behavior [13,95,96]. Finally, it is worth studying how the nonequilibrium dynamics of generalized AAH models, for instance, quasiperiodic modulation of hopping and on-site potential [24], will follow the KZM scaling hypothesis and display signatures of dynamical quantum phase transitions captured by the Loschmidt echo dynamics.

ACKNOWLEDGMENTS

This work is supported by NSF of China (Grants No. 11835011 and No. 11774316) and Zhejiang Provincial Ten Thousand Talent Program (Grant No. 2017R52046).

APPENDIX A: LOSCHMIDT ECHO IN TWO LIMITED CASES

Firstly, V_i is set to 0 and the system is initially prepared in the extended phase with periodic boundary condition, that is, a plane wave state is the eigenstate of the Hamiltonian:

$$|\phi_k(V_i = 0)\rangle = \frac{e^{-i\pi/4}}{\sqrt{N}} \sum_{j=1}^{N} e^{ikj} c_j^\dagger |0\rangle, \tag{A1}$$

where the wave vector $k = \frac{2\pi(l-\frac{N}{2})}{aN} \in (-\frac{\pi}{a}, \frac{\pi}{a}]$ $(l = 1, \ldots, N)$ in the Brillouin zone. With the eigenvalues ε_k of the initial Hamiltonian $H(V_i)$:

$$\varepsilon_k = 2\sqrt{(J\cos ka)^2 + (\Delta \sin ka)^2}. \tag{A2}$$

When $V_f \to \infty$, the eigenstates of the Hamiltonian become

$$|\Psi_n(V_f = \infty)\rangle = \sum_{j=1}^{N} \delta_{jn} c_j^\dagger |0\rangle. \tag{A3}$$

Here, $|\Psi_n(V_f)\rangle$ represents the $n-$th eigenstates of the quenched Hamiltonian. The corresponding eigenvalue ε_n of the quenched Hamiltonian is

$$\varepsilon_n = V_f \cos(2\pi\alpha n). \tag{A4}$$

For a sudden quench, the system crosses from the initial value V_i to final value V_f. For simplicity, we use the $|k\rangle$ to replace $|\phi_k(V_i = 0)\rangle$. So substituting Eqs. (A1), (A3), and (A4) into Eq. (18), the return amplitude can rewritten as

$$\begin{aligned} G_k(t) &= \langle k|e^{-iH(V_f)t}|k\rangle \\ &= \sum_n \langle k|e^{-iH(V_f)t}|\Psi_n(V_f)\rangle\langle\Psi_n(V_f)|k\rangle \\ &= \sum_n e^{-i\varepsilon_n t}|\langle\Psi_n(V_f)|k\rangle|^2 \\ &= \frac{1}{N}\sum_{n=1} e^{-iV_f t\cos(2\pi\alpha n)}. \end{aligned} \tag{A5}$$

Because of the irrational number α, the phase $2\pi\alpha n$ $(n = 1, \ldots, N)$ modulus 2π is set randomly between $-\pi$ and π when we sum over from 1 to the large N. So we can approximately replace the summation by the integration

$$G_k(t) \approx \frac{1}{2\pi}\int_{-\pi}^{\pi} e^{-iV_f t\cos\theta} d\theta = J_0(V_f t), \tag{A6}$$

where the $J_0(V_f t)$ is the zero-order Bessel function. According to the nature of Bessel function, we know that the zero-order Bessel function $J_0(x)$ has a series zero-point x_n with $n = 1, 2, 3, ...$ In the first case, the Loschmidt echo will reach zero at times:

$$t_n^* = \frac{x_n}{V_f}. \tag{A7}$$

Conversely, we consider another limit, the quenching process from a strong disorder strength $V_i \to \infty$ to the final $V_f = 0$. By substituting Eqs. (A1), (A3), and (A2) into Eq. (18), we can get the return amplitude:

$$\begin{aligned} G_n(t) &= \langle n|e^{-iH(V_f)t}|n\rangle \\ &= \sum_k \langle n|e^{-2it\sqrt{(J\cos ka)^2+(\Delta\sin ka)^2}}|k\rangle\langle k|n\rangle \\ &= \sum_k e^{-2it\sqrt{(J\cos ka)^2+(\Delta\sin ka)^2}}|\langle k|n\rangle|^2 \\ &= \frac{1}{N}\sum_k e^{-2it\sqrt{(J\cos ka)^2+(\Delta\sin ka)^2}}, \end{aligned} \tag{A8}$$

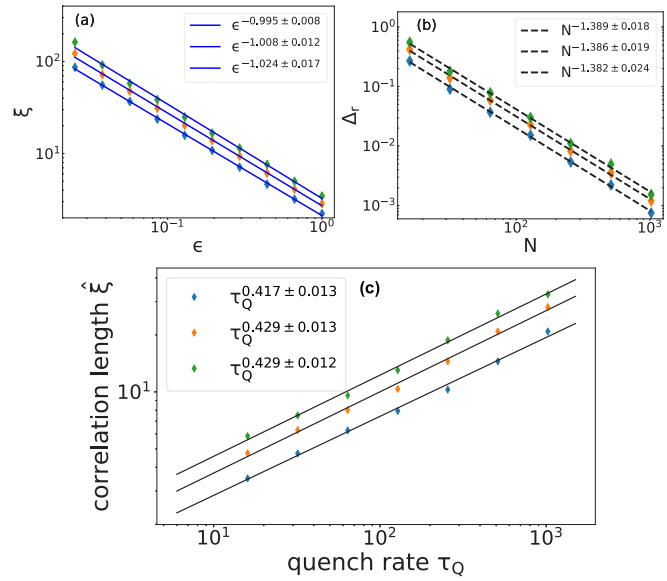

FIG. 8. Similar calculations are shown as those in Figs. 2 and 4 with different critical points. (a) The localization length ξ as a function of the distance from the critical point $\epsilon = V - V_c$. The linear fit yields correlation-length exponents $\nu = 0.995 \pm 0.008,\ 1.008 \pm 0.012,\ 1.024 \pm 0.017$. (b) The relevant gap Δ_r at the critical points as a function of system size N. The dynamical exponents $z = 1.389 \pm 0.018,\ 1.386 \pm 0.019,\ 1.382 \pm 0.024$ are obtained from the power-law fitting. (c) The width of the wave packet as a function of the quench time τ_Q at the critical point. The fitting straight lines give $\hat{\xi} = \tau_Q^{0.417\pm0.013}$, $\hat{\xi} = \tau_Q^{0.429\pm0.013}$, $\hat{\xi} = \tau_Q^{0.429\pm0.012}$ for the critical points at $(\Delta, V_c) = (0.4, 2.8)$, $(0.8, 3.6)$, and $(1.2, 4.4)$, respectively. The parameters are chosen as $N = 987$ and $\phi = 0$.

where $|n\rangle$ denotes $|\Psi_n(V_i = \infty)\rangle$. When $\Delta \ll J$ and in the large N limit, the sum can be transformed into an integral. The same is true for $\Delta \gg J$

$$\begin{aligned} G_n(t) &= \frac{a}{2\pi}\int_{-\frac{\pi}{a}}^{\frac{\pi}{a}} e^{-2iJt\cos ka} dk \\ &= J_0(2Jt). \end{aligned} \tag{A9}$$

Therefore, the Loschmidt echo gets zero at times:

$$t_n^* = \frac{x_n}{2J}, \tag{A10}$$

which are $1/2J$ of the zeros of the zero-order Bessel function $J_0(x)$, different from Eq. (A7).

APPENDIX B: ADIABATIC QUENCH FOR OTHER CRITICAL POINTS

We proceed to investigate the adiabatic quench for three other critical points, $V_c = 2.8, 3.6, 4.4$. Furthermore, for the sake of completeness, we calculate the critical behavior of the correlation function and the relevant gap near the critical points. In Fig. 8(a), we plot the localization length ξ as a function of the distance from the critical point $\epsilon = V - V_c$ at $\Delta = 0.4, 0.8, 1.2$. The linear fit to the log-log plot yields the correlation length exponent $\nu = 0.995 \pm 0.008,\ 1.008 \pm 0.012,\ 1.024 \pm 0.017$. At $\Delta = 0.4,\ 0.8,1.2$, the relevant gap as a function of system size N is shown in Fig. 8(b).

And the corresponding dynamical exponent is $z = 1.389 \pm 0.018$, 1.386 ± 0.019, 1.382 ± 0.024.

Figure 8(c) displays the width of the evolving state at the critical point $\epsilon = 0$ as a function of τ_Q at these critical points. The power-law fitting leads to $z = 1.393$ for $\nu = 0.995$, $z = 1.339$ for $\nu = 1.008$, $z = 1.354$ for $\nu = 1.024$. Their average $z = 1.362$ is 1% below the $z = 1.373$ obtained from the finite-size scaling in Fig. 2(b). Therefore, the numerical results are in a good agreement with the predicted ones, and the universality of the KZM theory on the second-order phase transition line is verified.

APPENDIX C: KZM IN A NONLINEAR QUENCH

The adiabatic-diabatic-adiabatic approximation in Sec. III can be extended to nonlinear quench,

$$\epsilon(t) \approx -\text{sign}(t)\left|\frac{t}{\tau_q}\right|^r \tag{C1}$$

at the critical point $\epsilon = 0$, where r is the adiabatic quench index with $r = 1$ the linear quench and $r \neq 1$ the nonlinear one. This function for $r \neq 1$ cannot be linearized like Eq. (12). However, essentially the same argument on the localization length can be applied as that in the case of linearity. In the following calculation, we will test $r = 1/2$.

Actually, the reaction time $\frac{1}{\Delta_r} \sim |\epsilon|^{-z\nu}$ equals the time scale $|\epsilon/\dot{\epsilon}|$ at $\hat{\epsilon} \sim (r/\tau_Q)^{r/(1+rvz)}$ corresponding to the KZ localization length,

$$\hat{\xi} \sim \tau_Q^{\frac{r\nu}{1+rvz}}. \tag{C2}$$

We compare these static predictions with the numerical results with a nonlinear quench starting from $t_i = -\tau_Q$. In Fig. 9, we plot the width of the evolution wave packet at the critical point as a function of τ_Q. The power-law fitting implies $z = 1.390$ for $\nu = 0.997$ (while $z = 1.396$ for $\nu = 1$).

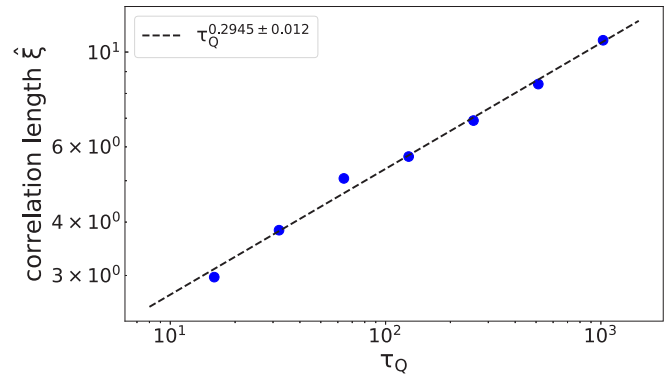

FIG. 9. The width of the wave packet as a function of the quench time τ_Q at the critical point $\epsilon = 0$ for generalized nonlinear power-law protocols. The fitted straight line gives the $\hat{\xi} = \tau_Q^{0.2945 \pm 0.012}$; cf. Eq. (14) with $r = 1/2$. The parameters are chosen as $N = 987$, $\Delta = 0.5$, $V_c = 3$, and $\phi = 0$.

We extract the values of ν and z separately by combining two different quenches. x_1 is obtained by a linear quench for $r = 1$, $\nu/(1 + z\nu) = x_1$, and x_2 from a nonlinear quench with $r = 1/2$, $r\nu/(1 + rz\nu) = \nu/(2 + z\nu) = x_2$. Combine these two equations together,

$$\nu = \frac{x_1 x_2}{x_1 - x_2}, \quad z = \frac{2x_2 - x_1}{x_1 x_2}. \tag{C3}$$

The power-law fit implies the $x_2 = 0.2945$ estimated in Fig. 9, and $x_1 = 0.422$ estimated in Fig. 4. Substituting x_1, x_2 into Eq. (C3), we get $\nu = 0.975$, $z = 1.344$. So this method can be used to extract the dynamical exponent z independently [87], without knowing ν.

[1] M. Kohmoto, L. P. Kadanoff, and C. Tang, Localization Problem in One Dimension: Mapping and Escape, Phys. Rev. Lett. **50**, 1870 (1983).

[2] S. Ostlund, R. Pandit, D. Rand, H. J. Schellnhuber, and E. D. Siggia, One-Dimensional Schrödinger Equation with an Almost Periodic Potential, Phys. Rev. Lett. **50**, 1873 (1983).

[3] M. Kohmoto and J. R. Banavar, Quasiperiodic lattice: Electronic properties, phonon properties, and diffusion, Phys. Rev. B **34**, 563 (1986).

[4] J. Q. You, J. R. Yan, T. Xie, X. Zeng, and J. X. Zhong, Generalized Fibonacci lattices: Dynamical maps, energy spectra and wavefunctions, J. Phys.: Condens. Matter **3**, 7255 (1991).

[5] J. H. Han, D. J. Thouless, H. Hiramoto, and M. Kohmoto, Critical and bicritical properties of Harper's equation with next-nearest-neighbor coupling, Phys. Rev. B **50**, 11365 (1994).

[6] F. Liu, S. Ghosh, and Y. D. Chong, Localization and adiabatic pumping in a generalized Aubry-André-Harper model, Phys. Rev. B **91**, 014108 (2015).

[7] F. Igloi, Quantum ising model on a quasiperiodic lattice, J. Phys. A **21**, L911 (1988).

[8] F. Iglói, L. Turban, D. Karevski, and F. Szalma, Exact renormalization-group study of aperiodic ising quantum chains and directed walks, Phys. Rev. B **56**, 11031 (1997).

[9] F. Iglói, R. Juhász, and Z. Zimborás, Entanglement entropy of aperiodic quantum spin chains, Europhys. Lett. **79**, 37001 (2007).

[10] F. Iglói, G. Roósz, and Y-C Lin, Non-equilibrium quench dynamics in quantum quasicrystals, New J. Phys. **15**, 023036 (2013).

[11] P. J. D. Crowley, A. Chandran, and C. R. Laumann, Quasiperiodic Quantum Ising Transitions in 1D, Phys. Rev. Lett. **120**, 175702 (2018).

[12] P. J. D. Crowley, A. Chandran, and C. R. Laumann, Critical behavior of the quasiperiodic quantum Ising chain, arXiv:1812.01660.

[13] U. Agrawal, S. Gopalakrishnan, and R. Vasseur, Universality and quantum criticality in quasiperiodic spin chains, Nat. Commun. **11**, 2225 (2020).

[14] P. G. Harper, Single band motion of conduction electrons in a uniform magnetic field, Proc. Phys. Soc. London Sect. A **68**, 874 (1955).

[15] H. Hiramoto and M. Kohmoto, Electronic spectral and wavefunction properties of one-dimensional quasiperiodic systems: A scaling approach, Int. J. Mod. Phys. B **06**, 281 (1992).
[16] M. Kohmoto, Metal-Insulator Transition and Scaling for Incommensurate Systems, Phys. Rev. Lett. **51**, 1198 (1983).
[17] D. J. Thouless, Bandwidths for a quasiperiodic tight-binding model, Phys. Rev. B **28**, 4272 (1983).
[18] H. Hiramoto and M. Kohmoto, Scaling analysis of quasiperiodic systems: Generalized harper model, Phys. Rev. B **40**, 8225 (1989).
[19] T. Geisel, R. Ketzmerick, and G. Petschel, New Class of Level Statistics in Quantum Systems with Unbounded Diffusion, Phys. Rev. Lett. **66**, 1651 (1991).
[20] I. Chang, K. Ikezawa, and M. Kohmoto, Multifractal properties of the wave functions of the square-lattice tight-binding model with next-nearest-neighbor hopping in a magnetic field, Phys. Rev. B **55**, 12971 (1997).
[21] Y. Takada, K. Ino, and M. Yamanaka, Statistics of spectra for critical quantum chaos in one-dimensional quasiperiodic systems, Phys. Rev. E **70**, 066203 (2004).
[22] J. Wang, X.-J. Liu, G. Xianlong, and H. Hu, Phase diagram of a non-Abelian Aubry-André-Harper model with *p*-wave superfluidity, Phys. Rev. B **93**, 104504 (2016).
[23] P. W. Anderson, Absence of diffusion in certain random lattices, Phys. Rev. **109**, 1492 (1958).
[24] Q.-B. Zeng, S. Chen, and R. Lü, Generalized Aubry-André-Harper model with *p*-wave superconducting pairing, Phys. Rev. B **94**, 125408 (2016).
[25] V. Khemani, D. N. Sheng, and D. A. Huse, Two Universality Classes for the Many-Body Localization Transition, Phys. Rev. Lett. **119**, 075702 (2017).
[26] M. M. Doria and I. I. Satija, Quasiperiodicity and Long-Range Order in a Magnetic System, Phys. Rev. Lett. **60**, 444 (1988).
[27] V. G. Benza, Quantum Ising quasi-crystal, Europhys. Lett. **8**, 321 (1989).
[28] M. M. Doria, F. Nori, and I. I. Satija, Thue-Morse quantum Ising model, Phys. Rev. B **39**, 6802 (1989).
[29] V. G. Benza, M. Kolár, and M. K. Ali, Phase transition in the generalized Fibonacci quantum Ising models, Phys. Rev. B **41**, 9578 (1990).
[30] J. M. Luck, Critical behavior of the aperiodic quantum Ising chain in a transverse magnetic field, J. Stat. Phys. **72**, 417 (1993).
[31] J. Hermisson, U. Grimm, and M. Baake, Aperiodic Ising quantum chains, J. Phys. A **30**, 7315 (1997).
[32] J. Hermisson and U. Grimm, Surface properties of aperiodic Ising quantum chains, Phys. Rev. B **57**, R673 (1998).
[33] J. M. Luck and T. M. Nieuwenhuizen, A soluble quasi-crystalline magnetic model: The XY quantum spin chain, Europhys. Lett. **2**, 257 (1986).
[34] I. I. Satija and M. M. Doria, Localization and long-range order in magnetic chains, Phys. Rev. B **39**, 9757 (1989).
[35] J. Hermisson, Aperiodic and correlated disorder in XY chains: Exact results, J. Phys. A **33**, 57 (1999).
[36] S. Xu, X. Li, Y.-T. Hsu, B. Swingle, and S. Das Sarma, Butterfly effect in interacting Aubry-Andre model: Thermalization, slow scrambling, and many-body localization, Phys. Rev. Research **1**, 032039(R) (2019).
[37] S. Katsura, Statistical mechanics of the anisotropic linear Heisenberg model, Phys. Rev. **127**, 1508 (1962).
[38] E. R. Smith, One-dimensional XY model with random coupling constants. I. Thermodynamics, J. Phys. C **3**, 1419 (1970).
[39] J. H. H. Perk, H. W. Capel, M. J. Zuilhof, and T. J. Siskens, On a soluble model of an antiferromagnetic chain with alternating interactions and magnetic moments, Physica A **81**, 319 (1975).
[40] H. Nishimori, One-dimensional XY model in lorentzian random field, Phys. Lett. A **100**, 239 (1984).
[41] O. Derzhko and J. Richter, Solvable model of a random spin-XY chain, Phys. Rev. B **55**, 14298 (1997).
[42] I. I. Satija, Symmetry breaking and stabilization of critical phase, Phys. Rev. B **48**, 3511 (1993).
[43] I. I. Satija and J. C. Chaves, XY-to-Ising crossover and quadrupling of the butterfly spectrum, Phys. Rev. B **49**, 13239 (1994).
[44] M. Heyl, A. Polkovnikov, and S. Kehrein, Dynamical Quantum Phase Transitions in the Transverse-Field Ising Model, Phys. Rev. Lett. **110**, 135704 (2013).
[45] C. Karrasch and D. Schuricht, Dynamical phase transitions after quenches in nonintegrable models, Phys. Rev. B **87**, 195104 (2013).
[46] E. Canovi, P. Werner, and M. Eckstein, First-Order Dynamical Phase Transitions, Phys. Rev. Lett. **113**, 265702 (2014).
[47] F. Andraschko and J. Sirker, Dynamical quantum phase transitions and the Loschmidt echo: A transfer matrix approach, Phys. Rev. B **89**, 125120 (2014).
[48] M. Heyl, Dynamical Quantum Phase Transitions in Systems with Broken-Symmetry Phases, Phys. Rev. Lett. **113**, 205701 (2014).
[49] M. Heyl, Scaling and Universality at Dynamical Quantum Phase Transitions, Phys. Rev. Lett. **115**, 140602 (2015).
[50] R. A. Jalabert and H. M. Pastawski, Environment-Independent Decoherence Rate in Classically Chaotic Systems, Phys. Rev. Lett. **86**, 2490 (2001).
[51] H. T. Quan, Z. Song, X. F. Liu, P. Zanardi, and C. P. Sun, Decay of Loschmidt Echo Enhanced by Quantum Criticality, Phys. Rev. Lett. **96**, 140604 (2006).
[52] R. Jafari and H. Johannesson, Loschmidt Echo Revivals: Critical and Noncritical, Phys. Rev. Lett. **118**, 015701 (2017).
[53] T. Gorin, T. Prosen, T. H. Seligman, and M. Žnidarič, Dynamics of Loschmidt echoes and fidelity decay, Phys. Rep. **435**, 33 (2006).
[54] M. E. Fisher, in *Boulder Lectures in Theoretical Physics*, edited by E. Wesely (University of Colorado, Boulder, 1965), Vol. 7.
[55] J. C. Budich and M. Heyl, Dynamical topological order parameters far from equilibrium, Phys. Rev. B **93**, 085416 (2016).
[56] S. Vajna and B. Dóra, Topological classification of dynamical phase transitions, Phys. Rev. B **91**, 155127 (2015).
[57] S. Sharma, U. Divakaran, A. Polkovnikov, and A. Dutta, Slow quenches in a quantum Ising chain: Dynamical phase transitions and topology, Phys. Rev. B **93**, 144306 (2016).
[58] U. Bhattacharya and A. Dutta, Interconnections between equilibrium topology and dynamical quantum phase transitions in a linearly ramped Haldane model, Phys. Rev. B **95**, 184307 (2017).
[59] G. Roósz, U. Divakaran, H. Rieger, and F. Iglói, Nonequilibrium quantum relaxation across a localization-delocalization transition, Phys. Rev. B **90**, 184202 (2014).
[60] M. Anquez, B. A. Robbins, H. M Bharath, M. Boguslawski, T. M. Hoang, and M. S. Chapman, Quantum Kibble-Zurek

Mechanism in a Spin-1 Bose-Einstein Condensate, Phys. Rev. Lett. **116**, 155301 (2016).

[61] C. Meldgin, U. Ray, P. Russ, D. Chen, D. M. Ceperley, and B. DeMarco, Probing the Bose glass–superfluid transition using quantum quenches of disorder, Nat. Phys. **12**, 646 (2016).

[62] A. Keesling, A. Omran, H. Levine, H. Bernien, H. Pichler, S. Choi, R. Samajdar, S. Schwartz, P. Silvi, S. Sachdev, P. Zoller, M. Endres, M. Greiner, V. Vuletić, and M. D. Lukin, Quantum Kibble–Zurek mechanism and critical dynamics on a programmable Rydberg simulator, Nature (London) **568**, 207 (2019).

[63] H. Saito, Y. Kawaguchi, and M. Ueda, Kibble-Zurek mechanism in a quenched ferromagnetic Bose-Einstein condensate, Phys. Rev. A **76**, 043613 (2007).

[64] A. Sinha, M. M. Rams, and J. Dziarmaga, Kibble-Zurek mechanism with a single particle: Dynamics of the localization-delocalization transition in the Aubry-André model, Phys. Rev. B **99**, 094203 (2019).

[65] V. Mukherjee, U. Divakaran, A. Dutta, and D. Sen, Quenching dynamics of a quantum XY spin-$\frac{1}{2}$ chain in a transverse field, Phys. Rev. B **76**, 174303 (2007).

[66] C. Lee, Universality and Anomalous Mean-Field Breakdown of Symmetry-Breaking Transitions in a Coupled Two-Component Bose-Einstein Condensate, Phys. Rev. Lett. **102**, 070401 (2009).

[67] J. Xu, S. Wu, X. Qin, J. Huang, Y. Ke, H. Zhong, and C. Lee, Kibble-Zurek dynamics in an array of coupled binary Bose condensates, Europhys. Lett. **113**, 50003 (2016).

[68] T. W. B. Kibble, Topology of cosmic domains and strings, J. Phys. A **9**, 1387 (1976).

[69] T. W. B. Kibble, Some implications of a cosmological phase transition, Phys. Rep. **67**, 183 (1980).

[70] T. W. B. Kibble, Phase-transition dynamics in the laboratory and the universe, Phys. Today **60**(9), 47 (2007).

[71] M. M. Rams and B. Damski, Quantum Fidelity in the Thermodynamic Limit, Phys. Rev. Lett. **106**, 055701 (2011).

[72] C. De Grandi, A. Polkovnikov, and A. W. Sandvik, Microscopic theory of nonadiabatic response in real and imaginary time, J. Phys.: Condens. Matter **25**, 404216 (2013).

[73] N. Fläschner, D. Vogel, M. Tarnowski, B. S. Rem, D.-S. Lühmann, M. Heyl, J. C. Budich, L. Mathey, K. Sengstock, and C. Weitenberg, Observation of dynamical vortices after quenches in a system with topology, Nat. Phys. **14**, 265 (2018).

[74] X. Cai, L.-J. Lang, S. Chen, and Y. Wang, Topological Superconductor to Anderson Localization Transition in One-Dimensional Incommensurate Lattices, Phys. Rev. Lett. **110**, 176403 (2013).

[75] H.-Q. Wang, M. N. Chen, R. W. Bomantara, J. Gong, and D. Y. Xing, Line nodes and surface Majorana flat bands in static and kicked p-wave superconducting Harper model, Phys. Rev. B **95**, 075136 (2017).

[76] M. Yahyavi, B. Hetényi, and B. Tanatar, Generalized Aubry-André-Harper model with modulated hopping and p-wave pairing, Phys. Rev. B **100**, 064202 (2019).

[77] L.-J. Lang and S. Chen, Majorana fermions in density-modulated p-wave superconducting wires, Phys. Rev. B **86**, 205135 (2012).

[78] A. Chandran and C. R. Laumann, Localization and Symmetry Breaking in the Quantum Quasiperiodic Ising Glass, Phys. Rev. X **7**, 031061 (2017).

[79] J. Dziarmaga, Dynamics of a quantum phase transition in the random Ising model: Logarithmic dependence of the defect density on the transition rate, Phys. Rev. B **74**, 064416 (2006).

[80] A. P. Young and H. Rieger, Numerical study of the random transverse-field Ising spin chain, Phys. Rev. B **53**, 8486 (1996).

[81] T. Caneva, R. Fazio, and G. E. Santoro, Adiabatic quantum dynamics of a random Ising chain across its quantum critical point, Phys. Rev. B **76**, 144427 (2007).

[82] B.-B. Wei, Fidelity susceptibility in one-dimensional disordered lattice models, Phys. Rev. A **99**, 042117 (2019).

[83] J. C. C. Cestari, A. Foerster, M. A. Gusmão, and M. Continentino, Critical exponents of the disorder-driven superfluid-insulator transition in one-dimensional Bose-Einstein condensates, Phys. Rev. A **84**, 055601 (2011).

[84] E. Lieb, T. Schultz, and D. Mattis, Two soluble models of an antiferromagnetic chain, Ann. Phys. (NY) **16**, 407 (1961).

[85] D. Sen, K. Sengupta, and S. Mondal, Defect Production in Nonlinear Quench Across a Quantum Critical Point, Phys. Rev. Lett. **101**, 016806 (2008).

[86] S. Mondal, K. Sengupta, and D. Sen, Theory of defect production in nonlinear quench across a quantum critical point, Phys. Rev. B **79**, 045128 (2009).

[87] C.-W. Liu, A. Polkovnikov, and A. W. Sandvik, Dynamic scaling at classical phase transitions approached through nonequilibrium quenching, Phys. Rev. B **89**, 054307 (2014).

[88] W. H. Zurek, U. Dorner, and P. Zoller, Dynamics of a Quantum Phase Transition, Phys. Rev. Lett. **95**, 105701 (2005).

[89] P. Zanardi and N. Paunković, Ground state overlap and quantum phase transitions, Phys. Rev. E **74**, 031123 (2006).

[90] M. Kolodrubetz, B. K. Clark, and D. A. Huse, Nonequilibrium Dynamic Critical Scaling of the Quantum Ising Chain, Phys. Rev. Lett. **109**, 015701 (2012).

[91] S. Deng, G. Ortiz, and L. Viola, Dynamical non-ergodic scaling in continuous finite-order quantum phase transitions, Europhys. Lett. **84**, 67008 (2008).

[92] A. Francuz, J. Dziarmaga, B. Gardas, and W. H. Zurek, Space and time renormalization in phase transition dynamics, Phys. Rev. B **93**, 075134 (2016).

[93] A. Peres, Stability of quantum motion in chaotic and regular systems, Phys. Rev. A **30**, 1610 (1984).

[94] H. Yin, S. Chen, G. Xianlong, and P. Wang, Zeros of Loschmidt echo in the presence of Anderson localization, Phys. Rev. A **97**, 033624 (2018).

[95] A. Szabó and U. Schneider, Non-power-law universality in one-dimensional quasicrystals, Phys. Rev. B **98**, 134201 (2018).

[96] T. Cookmeyer, J. Motruk, and J. E. Moore, Critical properties of the ground-state localization-delocalization transition in the many-particle Aubry-André model, Phys. Rev. B **101**, 174203 (2020).